cloud temperature in the same channel, and must mean a substantial depressing or clearing of the clouds at the pole, since the cloud temperature rises much more than that of the overlying atmosphere. This, in turn, implies strong descending motion.

Apart from the pole itself, the most striking warm feature is seen at mid-latitudes on the right-hand side of Fig. 3. This is suggestive of the Y-shaped features that are prominent in ultraviolet pictures of the planet (*4*). If a correlation can be established, the infrared measurements will provide strong constraints on theories of the origin of the ultraviolet markings. In any event, the complex structure of the cloud top temperatures suggest, in general, an equally complex circulation pattern.

Theoretical models and measurements at levels near 150 km predict higher temperatures than those implied by the very low brightness temperatures we observe at 125 km. This result is almost certainly due to the breakdown of local thermodynamic equilibrium (LTE) at low pressures, rather than to kinetic temperatures lower than 170 K. Non-LTE conditions at these levels on Venus have been predicted theoretically (*4*). Below 110 km (pressures greater than 10^{-6} bar), the infrared brightness temperature may safely be interpreted in terms of kinetic temperature (*4*).

The higher temperatures observed at the pole relative to the equator imply either a substantial haze at high altitudes near the equator, or a real increase in gas temperature with latitude on constant pressure surfaces. Although the Mariner 10 and Pioneer Venus ultraviolet imaging experiments both report high equatorial hazes, these seem to be very tenuous even at visible wavelengths (*8*). It is unlikely that they could provide enough opacity at 12 μm to account for the large contrasts observed; further analysis is needed to confirm this. Higher polar stratospheric temperatures, relative to the equator, imply several constraints on the atmospheric dynamics. Any poleward transport of heat in the stratosphere must be thermally indirect, that is, against the temperature gradient. This type of situation is encountered in Earth's stratosphere, where the motions are driven from below. On Venus, the mean meridional circulation, planetary scale waves, and small-scale eddies may all play a role in transporting heat poleward.

In addition, if the zonal wind is cyclostrophically balanced (*9*), higher polar temperatures would imply that the strength of the zonal wind decreases with height in the stratosphere. Our preliminary data then indicate that the 4-day circulation falls off above the cloud tops and is much reduced by the 80 km level. Ground-based spectroscopic data (*10*) suggest that the zonal circulation also varies in both time and longitude. Continued VORTEX data should distinguish between symmetric Hadley circulations, tides locked to the solar heating, and time-varying eddies, in producing this effect.

F. W. TAYLOR, D. J. DINER
L. S. ELSON, M. S. HANNER
D. J. MCCLEESE, J. V. MARTONCHIK
P. E. REICHLEY
Earth and Space Sciences Division, Jet Propulsion Laboratory, California Institute of Technology, Pasadena 91103
J. T. HOUGHTON, J. DELDERFIELD
J. T. SCHOFIELD, S. E. BRADLEY
Department of Atmospheric Physics, University of Oxford, Oxford, England
A. P. INGERSOLL
Division of Geological and Planetary Sciences, California Institute of Technology, Pasadena 91125

References and Notes

1. F. W. Taylor, F. E. Vescelus, P. B. Forney, G. T. Foster, J. R. Locke, J. T. Houghton, J. Delderfield, J. T. Schofield, "Pioneer Venus orbiter infrared radiometer. I: Instrument description," in preparation.
2. F. W. Taylor, R. Beer, D. J. McCleese, J. V. Martonchik, M. S. Hanner, P. B. Forney, "The Pioneer Venus orbiter infrared radiometer. II: Calibration," in preparation.
3. L. V. Ksanformality, E. V. Dedova, L. F. Obukhova, V. M. Pokras, N. V. Temnaya, G. F. Filippov, *Sov. Astron.-AJ.* **20**, 476 (1976).
4. R. E. Dickenson, *J. Atmos. Sci.* **29**, 1531 (1972).
5. M. J. S. Belton, G. R. Smith, G. Schubert, A. Del Genio, *ibid.* **33**, 1394 (1976).
6. D. J. Diner, J. A. Westphal, F. P. Schloerb, *Icarus* **27**, 191 (1976).
7. D. J. Diner, "Simultaneous ultraviolet and infrared imaging of Venus," thesis (part 2), California Institute of Technology (1978).
8. B. O'Leary, *J. Atmos. Sci.* **32**, 1091 (1975).
9. C. Leovy, *ibid.* **30**, 1218 (1973).
10. W. A. Traub and N. P. Carleton, "Retrograde winds on Venus: Possible periodic variations," preprint.
11. The VORTEX investigator team thanks the engineers at the Jet Propulsion Laboratory and others who delivered the instrumentation, particularly B. Locke, P. Forney, and T. Foster; F. Vescelus for brilliant task management; and the personnel at Ames Research Center who monitored the instrument development and assisted with its successful implementation, particularly A. Wilhelmi, E. Tischler, J. Sperrans, and S. Hing. This report represents one phase of research carried out by JPL under NASA contract NAS 7-100; D.J.D. is a NASA-NRC resident research associate.

15 January 1979; revised 22 January 1979

Orbiter Cloud Photopolarimeter Investigation

Abstract. *The first polarization measurements of the orbiter cloud photopolarimeter have detected a planet-wide layer of submicrometer aerosols of substantial visible optical thickness, of the order of 0.05 to 0.1, in the lower stratosphere well above the main visible sulfuric acid cloud layer. Early images show a number of features observed by Mariner 10 in 1974, including planetary scale markings that propagate around the planet in the retrograde sense at roughly 100 meters per second and bright- and dark-rimmed cells suggesting convective activity at low latitudes. The polar regions are covered by bright clouds down to latitudes approximately 50 degrees, with both caps significantly brighter (relative to low latitudes) than the south polar cloud observed by Mariner 10. The cellular features, often organized into clusters with large horizontal scale, exist also at mid-latitudes, and include at least one case in which a cell cuts across the edge of the bright polar cloud of the northern hemisphere.*

One major objective of the orbiter cloud photopolarimeter (OCPP) experiment is to determine physical properties (size, shape, and refractive index) of the haze and cloud particles on Venus, and to measure the vertical distribution of these aerosols. The diurnal, altitudinal, and latitudinal variations obtained for these properties should contribute to our understanding of the processes of formation and decay of the aerosols that form a ubiquitous veil around Venus.

The second major objective is to obtain images in ultraviolet light and to use these to study large-scale cloud morphology, measure cloud-tracked winds, and determine characteristics of wave propagation in the atmosphere of Venus. The geometry for imaging from the orbiter will yield nearly full-disk images for approximately 80 days beginning in the middle of January 1979, thus permitting extension of the time scales for dynamical studies by an order of magnitude over that obtained by Mariner 10 imaging, which lasted for 8 days (*1*, *2*). The planned extended mission for Pioneer Venus will permit study of physical processes occurring on time scales up to several hundred Earth days (*3*–*7*).

The overall purpose of these studies is to better understand basic atmospheric and climatic processes. Improved knowledge of the life cycle of aerosols on Venus, together with analysis of their effect on atmospheric structure, may contribute to determination of the role of atmospheric aerosols in terrestrial climate. Similarly, the information obtained on the general circulation and

0036-8075/79/0223-0781$00.50/0

clouds should be valuable for basic dynamical studies. Venus provides a dynamical laboratory free of large Coriolis forces and heating contrasts between land and sea, as well as an excellent opportunity for studying global interactions of clouds, radiation, and climate.

The OCPP instrument uses a positionable 3.7 cm Cassegrain telescope, which provides viewing angles, as measured from the spacecraft spin axis, in the range 0° to 145°. The 5 rev/min spin rate of the spacecraft is used to scan the instrument field of view across the planet, while spacecraft orbital motion provides translation of the scan lines for two-dimensional coverage. A 16-position filter wheel, various optics, and photodiode detectors follow the telescope (*8*). Through the use of different wheel positions and appropriate instrument processing logic, measurements are made in one of three modes of operation: imaging, polarimetry, or limb-scan.

The imaging mode uses a 365-nm filter, a 0.4 by 0.45 mrad aperture, and a single photodiode detector; it yields scan lines of 1016 8-bit intensity measurements with a typical resolution of 30 km at the subspacecraft point. The spin-scan imaging technique with a single detector provides high photometric precision, which is valuable for quantitative analyses of vertical atmospheric structure as well as for maximum enhancement of features in the images. This technique also permits the high geometric fidelity needed for obtaining accurate cloud-tracked winds.

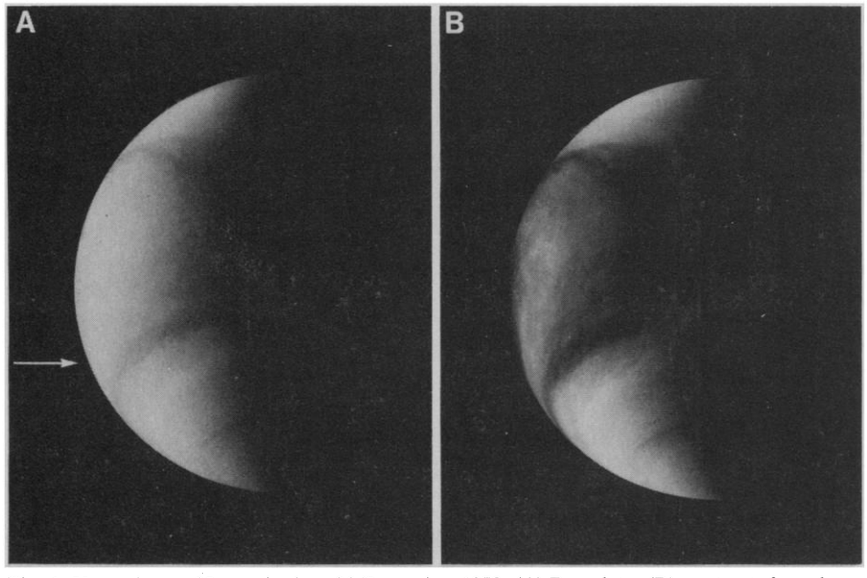

Fig. 1. Venus image 38 acquired on 25 December 1978. (A) Raw data; (B) contrasts have been enhanced. The morning terminator is on the right, and the subsolar point is just onto the bright limb, the phase angle being 88°. The south pole, on the terminator near the bottom of the picture, was scanned approximately 4 hours before the north polar region. The bright polar clouds in either hemisphere and the arms of the dark Y feature are visible in both versions of the image. A sharp dark collar exists around the southern polar cloud in the enhanced version. Bright streaky appendages on the equatorward periphery of the polar ring are similar to whorls and hooklike patterns in some Mariner 10 images.

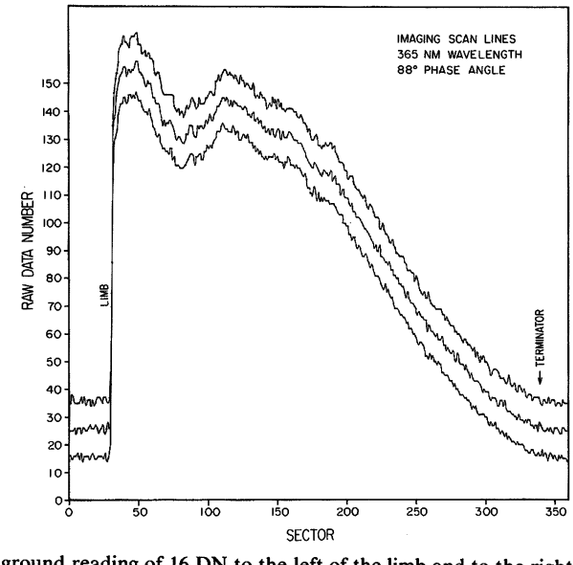

Fig. 2. Three consecutive scan lines across Venus, illustrating the geometric and photometric fidelity of the OCPP spin-scan system. The upper-two scan lines are shifted vertically by 10 and 20 data numbers. Note the sharp limb and the general gradient toward the terminator. These scans cross the southern hemisphere arm of the Y feature (Fig. 1), which is 18 percent darker than nearby cloud material, and many smaller features, some only one or two pixels (sectors) across, with contrasts of 2 percent or less. The signal-to-noise ratio is approximately 100. The instantaneous field of view was 26 km across (at the subspacecraft point). The scans were taken 12 seconds apart, corresponding to 10 km of cross-scan motion. The background reading of 16 DN to the left of the limb and to the right of the terminator is an instrumental offset.

In the polarimetry mode, the intensity, degree of linear polarization, and its azimuth are measured in four spectral bands: 270 nm (far ultraviolet), 365 nm (ultraviolet), 550 nm (visible), and 935 nm (near infrared), with three half-wave retarder positions on the filter wheel for each wavelength. The aperture size is 6.5 by 8 mrad, yielding a typical resolution of 250 to 500 km at the subspacecraft point. A Wollaston prism and two photodiode detectors analyze the filtered beam. Repeated observations of a given region make it possible to study the variation of the polarization with phase angle and zenith angle (*9*). The polarization as a function of phase angle and wavelength is used to obtain physical properties of aerosols and cloud particles (*10–12*). The polarization as a function of zenith angle and wavelength is used to measure pressure at the cloud top and the vertical distribution of aerosols (*12*).

The limb-scan measurements are obtained from scans of the OCPP field of view across the limb of the planet when the spacecraft is near periapsis (closest approach). This mode uses a 690-nm filter and an 0.3 by 0.35 mrad aperture to obtain an altitude resolution of about 1 km for latitudes within about 45° of periapsis (20°N). The limb-scan observations will be used to determine the vertical layering of high-altitude haze layers.

The three types of observations are complementary, with the information on aerosols and clouds from the polarization and limb-scan measurements helping to provide interpretation of what is observed in the images. In addition, the OCPP is designed so that it can be pointed to view either the area being observed by the ultraviolet spectrometer or the area being viewed by the infrared radiometer (*13*), thus permitting coordinated studies of atmospheric processes.

The OCPP data reduced to date are several images and polarization maps obtained from a direct tie-in to the NASA Deep Space Communications Network via a telephone circuit between Goddard Institute for Space Studies (in New York) and Goddard Space Flight Center

(in Greenbelt, Maryland). These are limited data intended for mission operations purposes; data analysis will depend upon the complete measurement records and accompanying spacecraft trajectory data, which are needed to produce geometrically rectified images, to determine precise angles for photometric and polarimetric analyses, and to obtain accurate cloud-tracked winds. However, to permit preliminary data analysis, the limited data for several images and polarization maps have been reduced and are presented here.

Imaging is performed at altitudes greater than ~ 33,000 km, when the spacecraft is moving sufficiently slowly that consecutive scan lines are contiguous or overlap. Since the spacecraft orbit has an eccentricity of 0.84 and an inclination of 105°, this technique restricts the images to the portion of the orbit for which the subspacecraft point ranges from 50°S to 24°N, while the longitude ranges over only 23°. Consequently, the phase angle, which specifies the amount of illumination of the disk, is similar for all images in a given orbit. The phase angle continuously changes at the rate of the apparent solar motion, 1.6° per day.

The first images were obtained at a phase angle of about 120°, when Venus appeared as a crescent with approximately one quarter of the disk illuminated. The dominant characteristic in the images at this angle is a steep gradient in intensity from the bright limb to the morning terminator. Intensities along individual scan lines contain variations superimposed on this large gradient, but the maximum contrast does not exceed approximately 5 percent. By comparison, images obtained by Mariner 10 at a phase angle of about 25° showed maximum contrasts of approximately 30 percent. The relatively low contrasts for oblique viewing conditions led us to the qualitative conclusion that the ultraviolet absorption responsible for dark features must lie beneath the topmost region of the bright sulfuric acid clouds. If the absorber were above the main visible cloud deck, the contrasts should be much larger than observed. This conclusion will be made quantitative from analysis of polarimetric and photometric data taken by the OCPP as the observing conditions range over all phase angles.

In more recently acquired images, at phase angles near 90°, the contrast has increased substantially. This is illustrated in Fig. 1, which shows Venus image 38 (*14*) obtained on 25 December at a phase angle of about 88° (*15*). Both the raw image data (Fig. 1A) and a version with contrast enhancement (Fig. 1B) are shown. Contrast enhancement is desirable to aid detailed examination of the images; this was true even for the Mariner 10 images which were taken at a small phase angle. The enhancement process used here was a "normalization" procedure similar to that employed by Limaye and Suomi (*16*), which consists of using a simple multiple scattering model to remove much of the large-scale variation in intensity caused by solar zenith angle variation over the disk.

The subspacecraft point for image 38 was at latitude 25°S and a longitude 89° east (upwind) of the subsolar point at the time of the midpoint of its acquisition. Thus this image presents a good view of the south polar region, which exhibits a circumpolar structure somewhat similar to that in Mariner 10 pictures, for which the spiral-shaped bright clouds have been described as a polar "ring" (*1*, *2*) or "vortex" (*17*). The brightest position in the polar ring is located near 50°S latitude, with considerable structure in the clouds poleward from the latitude. The arms of what appears to be the familiar dark, horizontal Y are also prominent in image 38.

Figure 2 shows the raw data for three consecutive scan lines of the 1237 scan lines in image 38. The relative displacement of consecutive scan lines in this image is slightly more than one-third of the instantaneous field of view. Thus, the repeatability of small-magnitude features is evidence that they are real and measurable with the OCPP. Therefore, we anticipate that significant detail can be brought out by selected filtering of different spatial frequencies in the image, a procedure that will be followed after the complete image and trajectory data become available.

Figure 3 shows an enhanced version of OCPP Venus image 45 acquired at a phase angle of 72°. The subspacecraft point is near 5°N, yielding comparable views of both hemispheres. Even without normalization, the regions at latitudes higher than 50° are brighter than any other points on the disk. This pronounced polar brightening has been noted in nearly all the OCPP images obtained to date. Although bright polar regions were evident in the Mariner 10 images, they became brighter than the lower-latitude regions only after the normalization performed by Limaye and

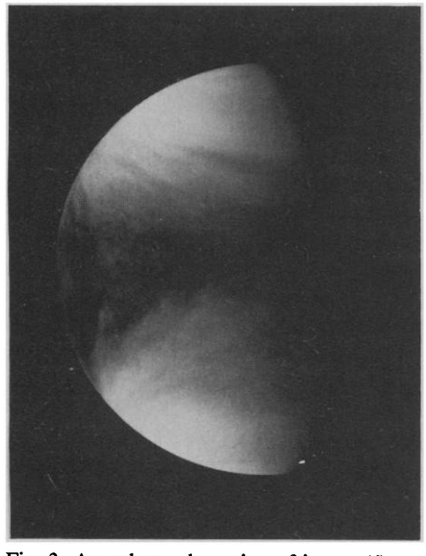

Fig. 3. An enhanced version of image 45 acquired about 5.5 days after image 38 at a phase angle of 72°. The subspacecraft point is about 5°N, so that the equator is approximately horizontal and near the center. The subsolar point is close to the equator near the almost vertical bands which are the bowlike waves. Cellular structure exists in the subsolar region. The polar clouds are exceptionally bright even without enhancement.

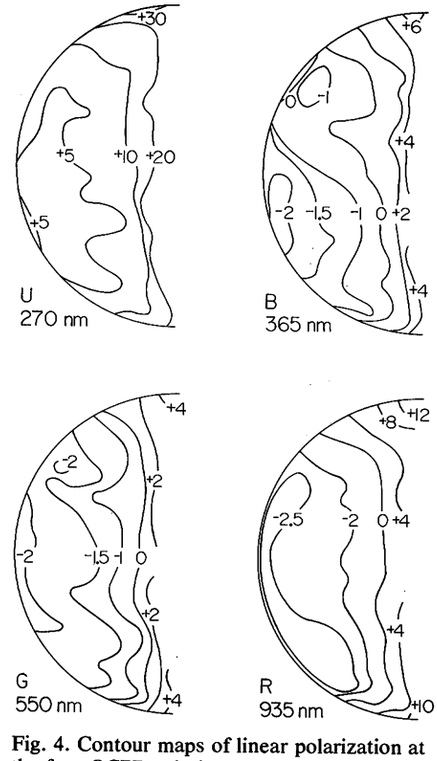

Fig. 4. Contour maps of linear polarization at the four OCPP polarimetry wavelengths. The observations were made on 13 December 1978, when the phase angle was 96° (*15*). The center of the visible disk is at 13°N latitude, with north at the top. The instantaneous field of view is approximately 280 km at the subspacecraft point. The positive polarization at 270 nm is produced by Rayleigh scattering from gas in and above the visible clouds. The negative polarization at the longer wavelengths is caused by sulfuric acid particles of 1 μm radius, while the positive values at the poles and terminator in the 935 nm map require the existence of a thin haze layer of small particles above the main cloud.

Suomi (*16*). For image 45, however, the southern polar region is 60 percent brighter than the equatorial region in the raw data. Thus, the present polar brightening is substantially greater than that occurring at the time of the Mariner 10 Venus encounter. Such a long-term variation is not particularly surprising in light of the history of variation noted in ground-based observations (*4*).

Several preliminary conclusions can be drawn from the first images, despite their large phase angles, the small number that have been reduced, the crudeness of the geometric rectification and contrast enhancement. The dark horizontal Y feature was apparent as early as 17 December and has since reappeared with an approximate 4-day period, consistent with previous observations (*1*, *2*, *18*). Images for times between the reappearances of the Y feature are characterized by the bright polar caps and a relatively dark region at low latitudes with occasional bright cloud features near the limb. Small bright appendages often trail out from the equatorward edge of the polar ring at substantial angles relative to parallels of latitude. Clear evidence of the retrograde motion of planetary scale and mesoscale features is also provided by pairs of images separated by 5 to 6 hours.

The OCPP images contain numerous examples of bright- and dark-rimmed cells suggestive of convective activity at low latitudes, similar to features observed from Mariner 10 (*1*). The enhanced images show cells organized into clusters with large horizontal scale. These cells exist even at mid-latitudes, including at least one cluster that cuts across the edge of the northern hemisphere bright polar cloud. Finally, OCPP images do contain features resembling the markings termed "bow-like waves" in Mariner 10 images.

The wavelength-dependent linear polarization for typical early measurements is shown in Fig. 4. Over most of the planet these results are consistent with the sulfuric acid cloud particles ($\sim$ 1-μm radius) identified from an analysis of ground-based polarimetry (*12*). However, the large positive (*19*) polarization near the terminator and cusp regions at 935 nm is much different from the strong negative polarization produced at this wavelength and phase angle by the 1-μm sulfuric acid cloud particles. A similar region of positive polarization (but of smaller magnitude) exists at the terminator and cusps at 550 nm.

These polarization characteristics imply the existence of an optically thin layer of small particles lying above the sulfuric acid clouds. This follows from the general behavior of the single scattering polarization as a function of particle size for phase angles 60° to 120° (*11*). For a given refractive index and particle radius (r) there is a specific particle size parameter ($x = 2\pi r/\lambda$) defining a boundary between positive and negative polarization. For a large range of sizes above this boundary value, the polarization is negative, whereas for smaller sizes it is increasingly positive. Thus, particles small enough to yield positive polarization at 935 nm, but not so small as to produce true Rayleigh scattering, will yield lower positive or even negative polarization at shorter wavelengths. Rayleigh scattering, such as by the molecular atmosphere above the clouds, cannot be responsible for the positive polarization at 935 nm. Because the optical thickness for Rayleigh scattering varies approximately as λ^{-4} (*11*), the amount of scattering required to produce the observed polarization at 935 nm would yield a far larger positive polarization at all the shorter wavelengths than is observed.

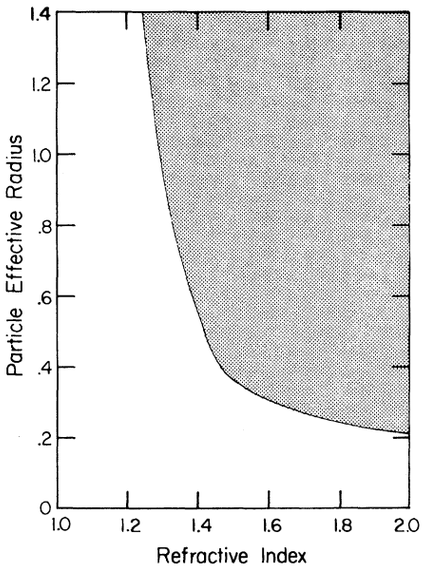

Fig. 5. Upper limit on particle size for the high-altitude haze layer. Particles within the shaded region would not produce the observed positive polarization at a phase angle of 96° and wavelength of 935 nm.

The upper boundary for the region of positive polarization depends upon the refractive index of the particles. After obtaining data from a broad range of phase angles, we should be able to determine the particle refractive index and an accurate value for the mean particle size. At present, we can specify an upper limit for the particle size (Fig. 5). If the refractive index of the particles in this upper haze layer is similar to that for the main cloud layer (1.44), the particles are not larger than 0.4 μm in radius. For any likely refractive index the particles are of submicrometer size (*20*).

The prevalence of positive polarization at 935 nm along the entire length of the terminator indicates that the haze layer is pervasive, at least in the morning sky of Venus. We have examined limited samples of polarimetry data acquired between 7 December 1978 and 5 January 1979, and find the same phenomenon in each instance.

It will be possible to determine the optical thickness and altitude of the upper-level haze from quantitative analyses of the polarization for all four wavelengths. The observed negative polarization over most of the disk at 935 nm indicates that it is possible to see through the small-particle haze layer for nongrazing solar incident angles. Estimates based on preliminary modeling suggest a vertical optical thickness of 0.05 to 0.1 in the visible region. The data at 270 nm will be used to determine the amount of gas above the haze layer, establishing its altitude relative to the tops of the sulfuric acid cloud; a very preliminary estimate places the haze in the stratosphere at roughly the 10-mbar level.

It is possible that this stratospheric haze layer varies significantly with time, for example, in its optical thickness. Its present optical thickness is sufficient to noticeably affect the disk-integrated polarization, which is known from Earth-based observations to change with time (*21*). We also note that there have been several suggestions for a haze layer above the visible clouds (*1*, *22*) and that it would be difficult to reconcile all the observations without invoking some time dependence for the haze. Pioneer Venus observations over two or three Venus years should provide valuable data for helping to unravel the processes determining the life cycle of the aerosols that compose the veil of haze blanketing Venus.

L. D. TRAVIS
D. L. COFFEEN
J. E. HANSEN
K. KAWABATA
A. A. LACIS
W. A. LANE
S. S. LIMAYE

NASA Goddard Institute for Space Studies, Goddard Space Flight Center, New York 10025

P. H. STONE

Department of Meteorology, Massachusetts Institute of Technology, Cambridge 02139

References and Notes

1. B. C. Murray *et al. Science* **183**, 1307 (1974).
2. M. J. S. Belton, G. R. Smith, D. A. Elliott, K. Klaasen, G. E. Danielson, *J. Atmos. Sci.* **33**, 1383 (1976); M. J. S. Belton, G. R. Smith, G. Schubert, A. D. Del Genio, *ibid.*, p. 1394.
3. Periods of nearly full-disk imaging will occur from the middle of August to the end of October 1979 and from the beginning of April to the middle of June 1980. Several reasons for anticipating that climate variations will be observable over a time scale of several hundred Earth days are: (i) ground-based ultraviolet images show major global changes on these time scales, such as the appearance or disappearance of a bright cloud covering either polar region (*4*); (ii) ground-based observations of the integrated disk polarization of Venus at 365 nm [figure 17 of (*5*)] show long-term variations in the mean contribution of Rayleigh scattering; (iii) the radiative time scale is tens to hundreds of days at the altitudes of the main clouds of Venus, 45 to 65 km (*6*); (iv) several cloud physics time scales are of the order of 10^7 seconds for particles of the size in the visible clouds of Venus (*7*).
4. A. Dollfus, *J. Atmos. Sci.* **32**, 1060 (1975).
5. D. L. Coffeen and J. E. Hansen, in *Planets, Stars, and Nebulae*, T. Gehrels, Ed. (Univ. of Arizona Press, Tucson, 1974), p. 518.
6. R. M. Goody and M. J. S. Belton, *Planet. Space Sci.* **15**, 247 (1967).
7. W. B. Rossow, *Icarus* **36**, 1 (1978).
8. The OCPP was built by Santa Barbara Research Center under specifications from the Goddard Institute for Space Studies. The instrument is described by E. Russell, L. Watts, S. Pellicori, and D. Coffeen [*Proc. Soc. Photo-Opt. Instrum. Eng.* **112**, 28 (1977)] and by L. Colin and D. M. Hunten [*Space Sci. Rev.* **20**, 451 (1977)].
9. The phase angle is the angle between the sun-planet and planet-observer directions, defined as zero for direct backscattering. The zenith angle is the angle between the local normal to the planetary surface and the direction of the sun (solar zenith angle) or the direction of observation.
10. The polarization as a function of phase angle and wavelength can be used to obtain the size, shape, and refractive index of aerosols. Quantitative discussions are given in (*5*), (*11*), and (*12*).
11. J. E. Hansen and L. D. Travis, *Space Sci. Rev.* **16**, 527 (1974).
12. J. E. Hansen and J. W. Hovenier, *J. Atmos. Sci.* **31**, 1137 (1974); K. Kawabata and J. E. Hansen, *ibid.* **32**, 1133 (1975).
13. The ultraviolet spectrometer has a fixed view direction 60° from the positive z (spin) axis, whereas the infrared radiometer has a fixed view direction of 45°.
14. Identification of OCPP images of Venus is by consecutive numbers in order of acquisition, starting with 1 for the first image acquired on 5 December 1978.
15. The phase angle specified for an image or polarimetry map is the value for disk center at the time the subspacecraft point was observed. Thus, the phase angle for a particular point on the disk at the time it was observed can be different because of the finite distance of the spacecraft from the planet and the finite time employed to acquire the image. The former effect is the larger, giving rise to a maximum difference equal to the angular radius of the planet which ranges from 5° to 9° for the portion of the orbit during which imaging is normally performed.
16. S. S. Limaye and V. E. Suomi, *J. Atmos. Sci.* **34**, 205 (1977).
17. V. E. Suomi and S. S. Limaye, *Science* **201**, 1009 (1978).
18. C. Boyer and P. Guerin, *Icarus* **11**, 338 (1969); R. F. Beebe, *ibid.* **17**, 602 (1972); A. H. Scott and E. J. Reese, *ibid.*, p. 589.
19. The polarization is positive if the intensity in the plane of scattering is smaller than that in the perpendicular plane. Thus, Rayleigh scattering is positive, while light scattered from aerosols may be positive or negative depending on the physical characteristics of the particles [compare with (*11*)].
20. The calculations for Fig. 5 are for spherical particles. Similar calculations of spheroids by S. Asano and M. Sato (personal communication) indicate substantial change only for very nonspherical shapes.
21. The polarization at $\lambda \sim 1$ μm has been anomalous at times; both the current values at 0.935 μm and some previous ground-based values at 0.99 μm [A. Dollfus and D. L. Coffeen, *Astron. Astrophys.* **8**, 251 (1970)] are well above the long-term mean. The polarization in the ultraviolet also shows strong temporal variations (*5*), as does the strength of the rainbow in the polarization at visible and shorter wavelengths. This could be due, for example, to changes in the main cloud or in the amount of blanketing by the stratospheric haze.
22. W. A. Lane, *Astron. J.*, in press; J. V. Martonchik and R. Beer, *J. Atmos. Sci.* **32**, 1151 (1975).

23. We thank the Santa Barbara Research Center for the detailed design, construction, and calibration of the orbiter cloud photopolarimeter, which has performed flawlessly. We are very grateful to R. Fimmel, S. Hing, B. Pittman, and others at the Pioneer Project Office, Ames Research Center, for implementing our command sequences to the OCPP, and W. B. Rossow for his comments on a draft of this paper. D.L.C. and W.A.L. were supported by NASA grant 33-015-165 to State University of New York at Stony Brook. S.S.L. was supported by a National Research Council postdoctoral research associateship.

16 January 1979

Infrared Image of Venus at the Time of Pioneer Venus Probe Encounter

Abstract. *An image of the infrared emission from the Earth-facing hemisphere of Venus was obtained at the time the Pioneer Venus probes penetrated the atmosphere. The thermal structure of the atmosphere at the 85-millibar level included regions of rapidly varying polar features, a solar-related postdawn warm area, and a nonsolar-fixed nighttime warm area. The probes succeeded in entering each of these three thermal regions.*

As part of a program of ground-based thermal observations of Venus designed to characterize the spatial and temporal extent of thermal emissions from the Venus clouds, we obtained a hemisphere-wide infrared view of the planet during the entry of the Pioneer Venus probes. The observations were made with a bolometric detector viewing through a filter with a 10.6- to 12.6-μm spectral pass-

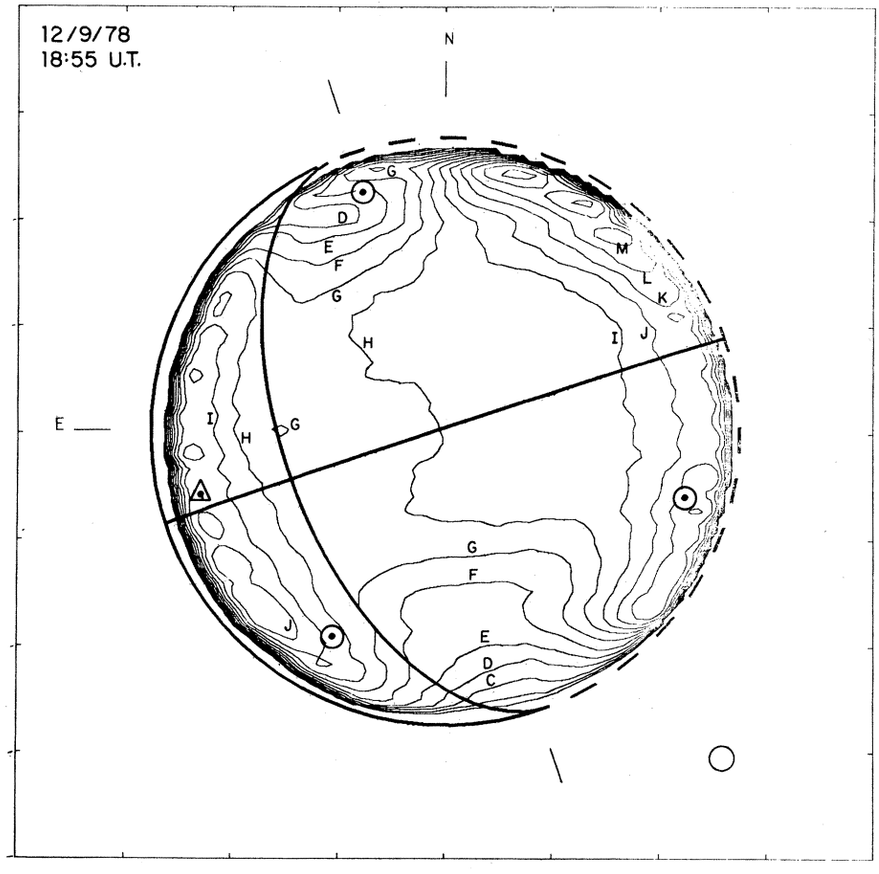

Fig. 1. Isophotal map of infrared emission from Venus at the time of probe entry with limb darkening removed. The radiance contours are equally spaced, by 2 percent of the average central intensity. Entry sites of small probes are indicated by circles, that of the large probe by a triangle. The dawn terminator, equator, and orientation of the Venus pole are shown, as are celestial north and east. The borders of the map enclosed a region measuring 64 by 64 arc seconds; the small circle in the lower right is the size of the detector aperture.

0036-8075/79/0223-0785$00.50/0